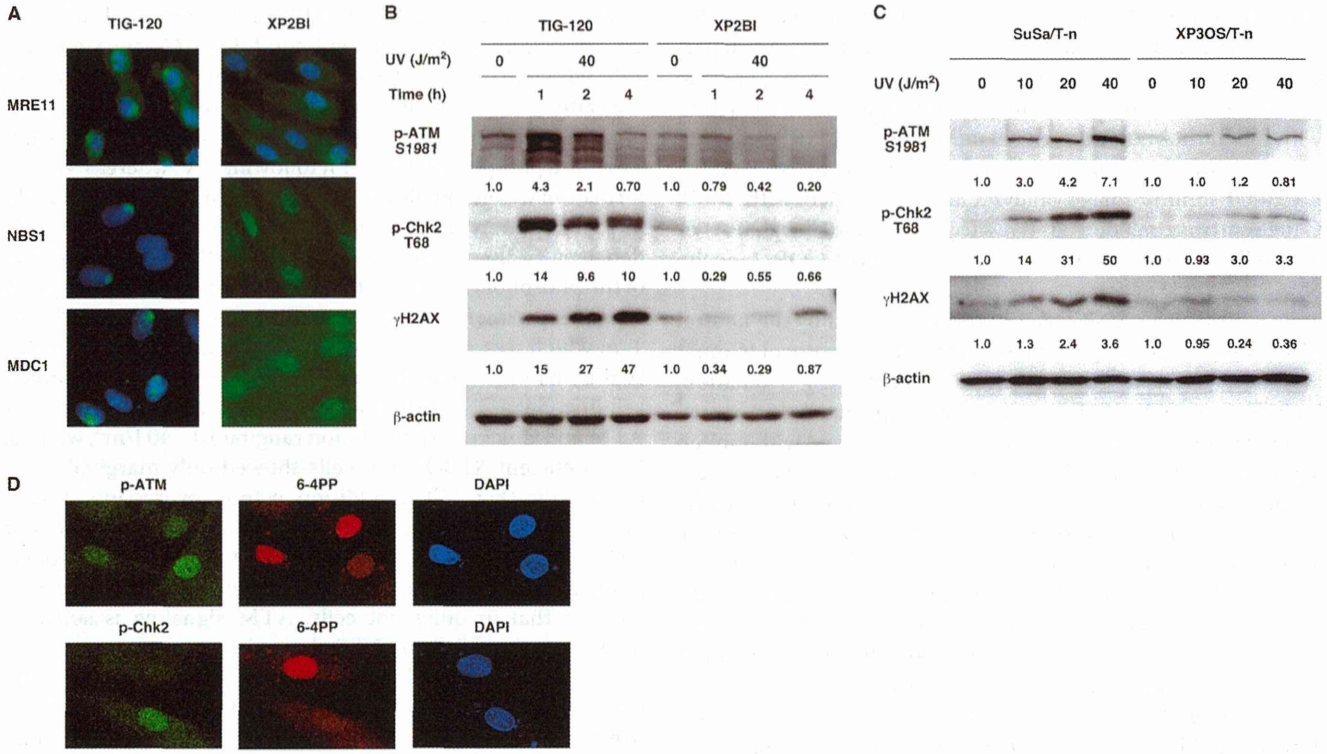

FIGURE 1. **NER-dependent recruitment of DDR factors and ATM activation in quiescent human cells.** *A*, TIG-120 or XP2BI cells were arrested in the G_0 phase by contact inhibition/serum starvation and locally irradiated with 40 J/m^2 of UV through an isopore membrane filter (pore size, 8 μm). After 1-h incubation, cells were fixed and stained with the indicated antibodies and DAPI. *B*, G_0-arrested TIG-120 or XP2BI cells were irradiated with 40 J/m^2 of UV and incubated for up to 4 h. Cell lysates were prepared and analyzed by Western blotting with the indicated antibodies. The relative signal intensities to unirradiated control were determined by Multi Gauge software and shown in the figure. *C*, G_0-arrested SuSa/T-n or XP3OS/T-n cells were irradiated with 10–40 J/m^2 of UV. After 1-h incubation, cell lysates were prepared and analyzed by Western blotting as described above. *D*, XP3OS/T-n cells were transfected with pCMV-Myc-XPA plasmid using FuGENE HD transfection reagent (Promega) and arrested in the G_0 phase by contact inhibition/serum starvation. At 2 h post-UV irradiation (40 J/m^2), the cells were fixed and double-stained with anti-6-4PP and anti-pATM (Ser^{1981}) or anti-pChk2 (Thr^{168}) antibodies.

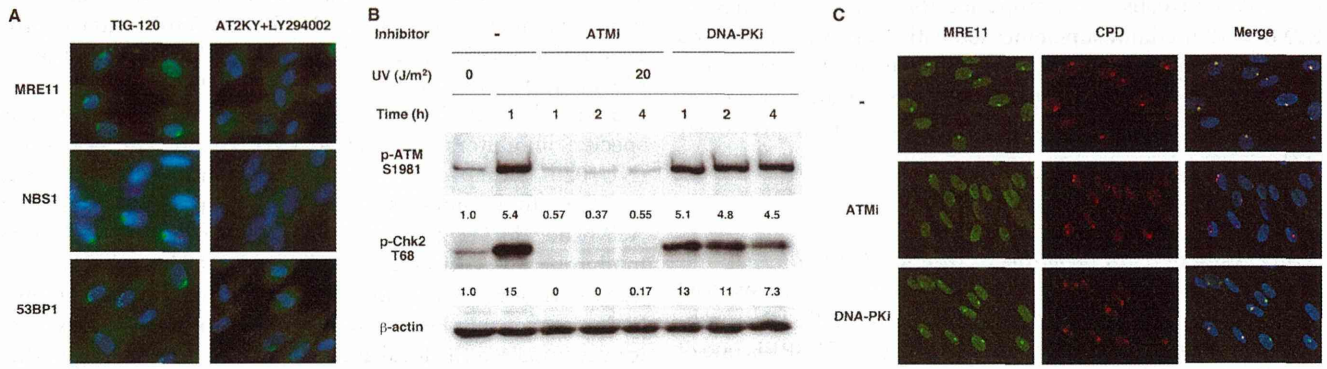

FIGURE 2. **The NER-dependent recruitment of DDR factors mainly depends on ATM activity.** *A*, TIG-120 or AT2KY cells were arrested in G_0 phase and locally irradiated with 40 J/m^2 of UV through an isopore membrane filter (pore size, 8 μm). After 1-h incubation, the cells were fixed and immunostained with the indicated antibodies. Note that AT2KY cells were treated with 100 μM LY294002 for 30 min before UV irradiation and during post-UV 1-h incubation. *B*, G_0-arrested TIG-120 cells were pretreated with or without either 10 μM KU-55933 (ATMi) or 10 μM NU7026 (DNA-PKi) for 30 min. The cells were irradiated with 20 J/m^2 of UV and incubated with or without each inhibitor for 1–4 h before cell lysis. The phosphorylation of ATM and Chk2 was analyzed by Western blotting with phospho-specific antibodies to Ser^{1981} and Thr^{68}, respectively. *C*, G_0-arrested TIG-120 cells were pretreated with ATMi or DNA-PKi as described above and locally irradiated with 40 J/m^2 of UV through an isopore membrane filter (pore size, 5 μm). After 1-h incubation with each inhibitor, the cells were co-immunostained with anti-MRE11 and anti-CPD antibodies.

(*A* and *B*), SuSa/T-n cells exhibited elongated comet tails following UV and a dose-dependent increase of tail moment. In clear contrast, NER-deficient XP3OS/T-n (XP-A) cells failed to show the elongation of comet tails (Fig. 3, *B* and *C*). These results strongly suggest that DSB is indeed generated in UV-irradiated quiescent cells in an NER-dependent manner.

ATM Partly Contributes to UV-induced H2AX Phosphorylation as Well as UV Resistance in Quiescent Human Cells—The findings of NER-dependent DSB formation and ATM activation 1 h post-UV in quiescent cells prompted us to test whether the early fraction of UV-induced H2AX phosphorylation is mediated by ATM. G_0-arrested TIG-120 cells were pretreated

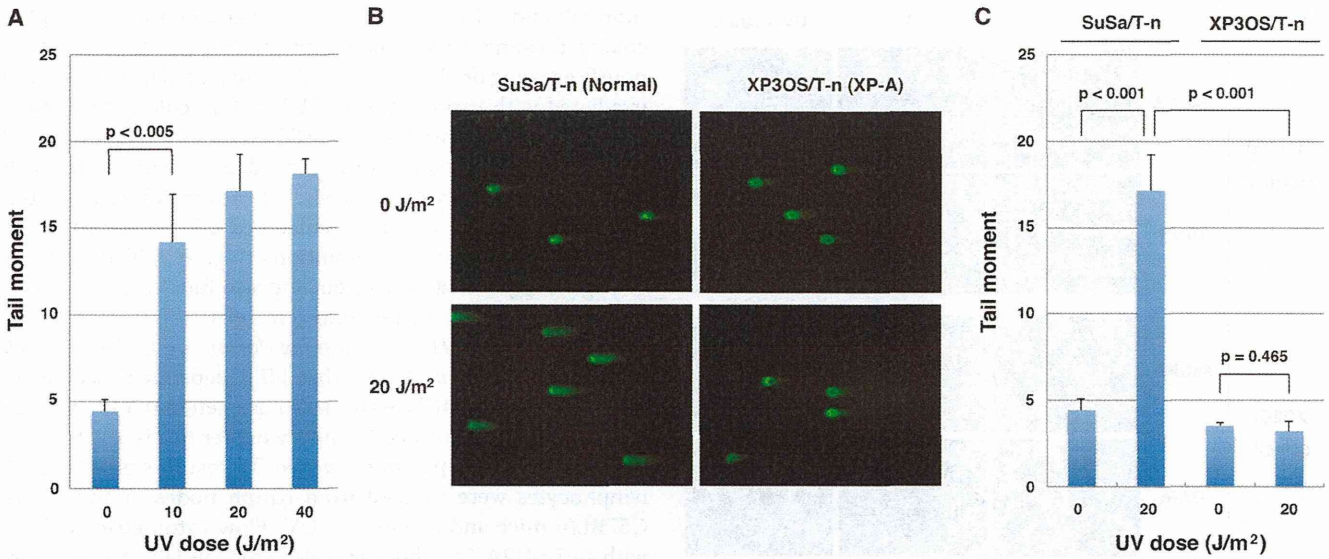

FIGURE 3. **NER-dependent DSB formation in quiescent human cells.** *A*, G_0-arrested SuSa/T-n cells were irradiated with the indicated doses of UV and incubated for 1 h. The cells were processed according to the manufacturer's instructions for the Comet assay kit (Trevigen), and tail moment was calculated using a CometScore™ program (TriTek Corp.). The mean values of tail moment with standard deviations were plotted as histograms. The statistical differences were determined by Student's *t* test. *B* and *C*, G_0-arrested SuSa/T-n or XP3OS/T-n cells were irradiated with 20 J/m² of UV and incubated for 1 h. DSB formation was analyzed by the neutral comet assay as described above. The representative images and quantitative data from three independent experiments were shown in *B* and *C*, respectively.

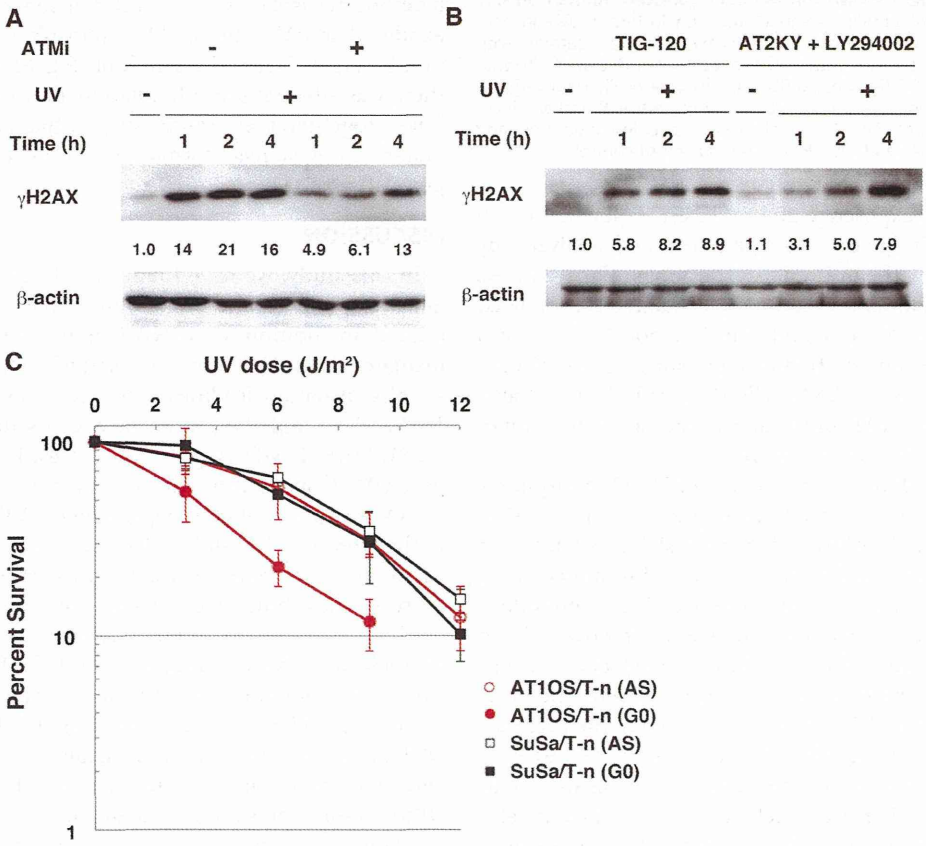

FIGURE 4. **Partial contribution of ATM to UV-induced H2AX phosphorylation and UV resistance in quiescent human cells.** *A*, G_0-arrested TIG-120 cells were pretreated with ATMi as described in the legend to Fig. 2 and irradiated with 20 J/m² of UV. After incubation with ATMi for the indicated periods, cell lysates were prepared and analyzed by Western blotting with anti-γH2AX antibody. *B*, G_0-arrested AT2KY cells were treated with LY294002 as described in Fig. 2. The cells were irradiated with 20 J/m² of UV, and the phosphorylation of H2AX was analyzed by Western blotting. *C*, asynchronously growing (*AS*) or G_0-arrested SuSa/T-n or AT1OS/T-n cells were plated into 60-mm dishes and irradiated with the indicated doses of UV after 6-h incubation. The cells were further incubated for 2–3 weeks, and the resultant colonies were counted after ethanol fixation and Giemsa staining.

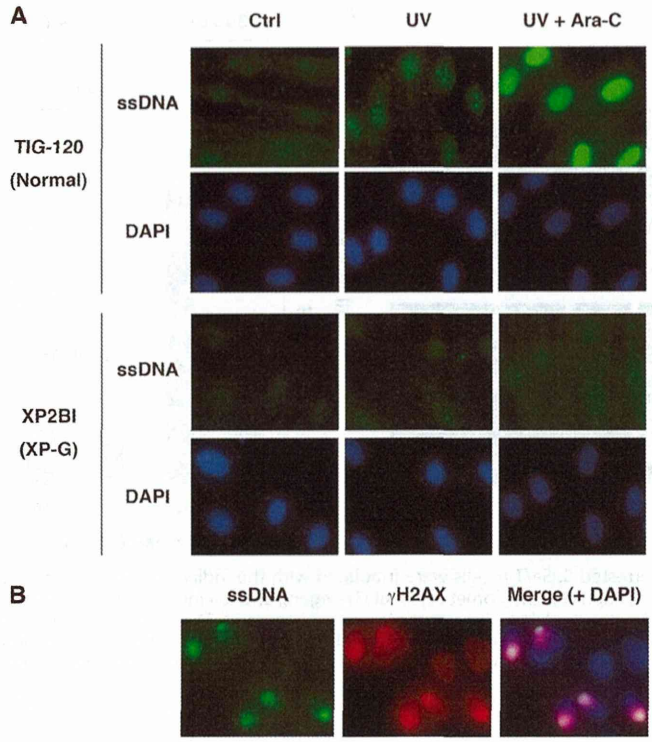

FIGURE 5. **NER-dependent ssDNA formation in quiescent human cells.** *A*, G_0-arrested TIG-120 or XP2BI cells were irradiated with 40 J/m^2 of UV and incubated for 4 h in the absence or presence of 100 μM Ara-C. After treatment with 0.5% Triton X-100, cells were fixed with methanol/acetone and stained with anti-ssDNA antibody and DAPI. *B*, G_0-arrested TIG-120 cells were locally irradiated with 40 J/m^2 of UV through an isopore membrane filter (pore size, 8 μm) and incubated for 4 h in the presence of Ara-C. The cells were fixed as described above and co-stained with anti-ssDNA and anti-γH2AX antibodies. *Ctrl*, control.

with KU-55933 and exposed to 20 J/m^2 of UV. Following 1–4 h of incubation, their lysates were prepared and analyzed by Western blotting with anti-γH2AX antibody (Fig. 4*A*). As expected, the ATM inhibitor markedly attenuated UV-induced H2AX phosphorylation at 1 and 2 h, but not 4 h. We also obtained the similar observation using a pair of TIG-120 cells and LY294002-treated AT2KY cells (Fig. 4*B*). These results clearly indicate that ATM contributes to the earlier fraction of UV-induced H2AX phosphorylation.

On the other hand, the latter fraction of H2AX phosphorylation (*i.e.* 4 h post-UV) is likely to be mediated by ATR in response to ssDNA (14). We tried to detect ssDNA formation in G_0-arrested TIG-120 cells exposed to UV by immunostaining with anti-ssDNA antibody. As shown in Fig. 5*A*, immunofluorescence signals in the nuclei were increased 4 h post-UV and further enhanced by the addition of Ara-C, which blocks a gap-filling step of NER. Importantly, those signals were undetectable in NER-deficient XP2BI (XP-G) cells even in the presence of Ara-C. In addition, locally UV-irradiated TIG-120 cells revealed that ssDNA regions are merged with γH2AX signals (Fig. 5*B*). Taken together, we conclude that in quiescent cells, NER reaction potentially generates at least two kinds of secondary DNA damage: DSB and ssDNA.

To explore the contribution of ATM signaling to UV resistance in quiescent cells, we employed a clonogenic survival assay. For this assay, hTERT-immortalized cell lines, SuSa/T-n (normal) and AT1OS/T-n (A-T), were used because of higher colony forming ability than primary fibroblasts. Asynchronously growing or G_0-arrested cells were plated into dishes and irradiated with various doses of UV before colony formation. Both cell lines showed similar UV sensitivity when exposed under asynchronously growing conditions, consistent with normal NER activity of A-T cells.[5] However, AT1OS/T-n but not SuSa/T-n cells exhibited enhanced UV sensitivity when exposed under quiescent conditions (Fig. 4*C*). These results strongly suggest that ATM signaling also functions in survival responses of UV-irradiated quiescent cells.

NER-dependent H2AX Phosphorylation in Quiescent Cell Populations in Vivo—Given that NER-dependent secondary DNA lesions (*i.e.* ssDNA and DSB) are generated in cultured quiescent cells, we wished to know whether this is also the case in quiescent cell populations *in vivo*. To test this possibility, T lymphocytes were isolated from lymph nodes or thymus of C57BL/6 mice and exposed to UV. Flow cytometric analyses with anti-γH2AX antibody revealed efficient H2AX phosphorylation in T lymphocytes from lymph nodes but not thymus, whereas etoposide-induced phosphorylation was comparably detected in both T cell populations (Fig. 6*A*). The inefficient H2AX phosphorylation in thymus-derived T lymphocytes might be explained by higher levels of DNA polymerase δ/ε and PCNA (Fig. 6*B*). On the other hand, lymph node-derived T lymphocytes isolated from NER-deficient xpa knock-out mice exhibited no UV-induced H2AX phosphorylation by flow cytometric (Fig. 6*C*) and Western blot (Fig. 6*D*) analyses, although there was efficient phosphorylation after etoposide treatment. Taken together, these results suggest that NER-dependent secondary DNA damage formation also occurs in quiescent cell populations *in vivo*.

DISCUSSION

In this study, we have found that DSB is also generated in quiescent cells exposed to UV in an NER-dependent manner (Fig. 3), in addition to ssDNA regions (Fig. 5) (14). The NER-mediated DSB formation is relatively rapid compared with ssDNA formation, leading to the activation of ATM kinase (Fig. 1, *B* and *C*) and the recruitment of its downstream factors, NBS1, MRE11, MDC1, and 53BP1 (Figs. 1*A* and 2*A*) within 1 h post-UV. Consistently, the earlier fraction of UV-induced H2AX phosphorylation is dependent on ATM activity (Fig. 4*A*). In the literature, UV-induced activation of ATM and its downstream reactions have been shown by several groups (25–27). In those studies, however, asynchronous cell populations were used, and thus the activation of ATM signaling is likely caused by replication fork stalling and/or DSB formation resulting from replication fork collapse, but not by NER.

Although NBS1, MRE11, MDC1, and 53BP1 are well known DDR factors involved in ATM signaling (2, 5, 21), they are also known to function in ATR signaling. The MRE11-RAD50-NBS1 complex acts both upstream and downstream of ATR to regulate the S phase checkpoint following UV (28). Moreover, Jeggo and co-workers (29) reported that replication-independent ATR signaling requires NBS1, 53BP1, and MDC1, but not H2AX, to induce G_2/M arrest. Recently, MDC1 was reported to accumulate at locally UV-damaged subnuclear regions in an

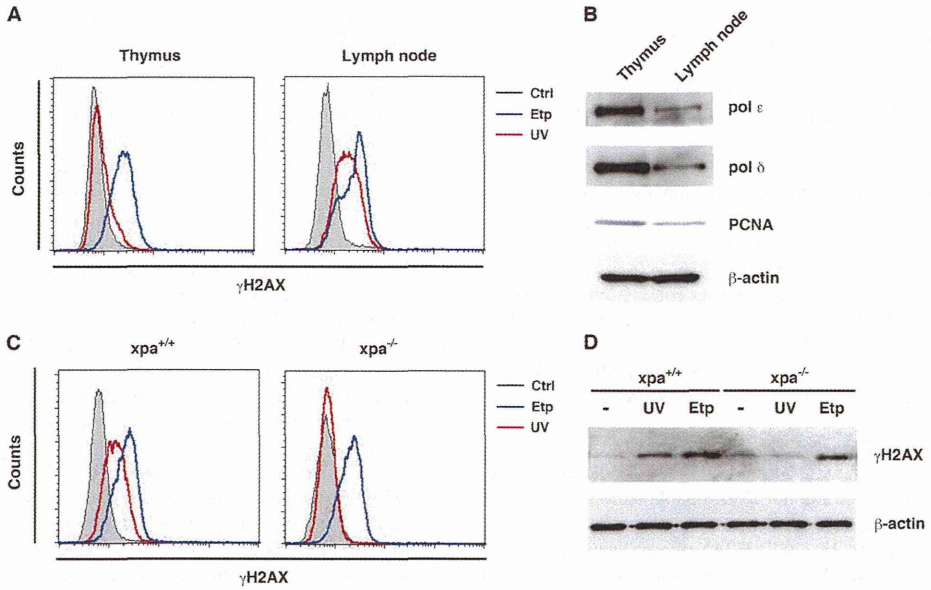

FIGURE 6. **UV-induced H2AX phosphorylation in peripheral T lymphocytes in an NER-dependent manner.** *A*, T lymphocytes isolated from thymus or lymph nodes of C57BL/6 mice were exposed to 20 J/m^2 of UV and incubated for 1 h or treated with 40 μg/ml of etoposide for 1 h. The cells were stained with anti-γH2AX antibody and propidium iodide and analyzed by flow cytometry. *B*, cell lysates were prepared from the isolated T lymphocytes and analyzed by Western blotting with the indicated antibodies. *C* and *D*, peripheral T lymphocytes from lymph nodes of wild-type or xpa knock-out mice were treated with UV or etoposide and analyzed for H2AX phosphorylation by flow cytometry (*C*) or Western blotting (*D*) with anti-γH2AX antibody. *Ctrl*, control; *Etp*, etoposide; *pol*, polymerase.

NER- and ATR-dependent manner, which recruits RNF8 ubiquitinating histone H2A and hereby 53BP1 and BRCA1 (30). In our experiments, however, local accumulation of MRE11 after micropore UV irradiation was markedly diminished by KU-55933 (Fig. 2*C*), suggesting downstream reactions of ATM signaling rather than ATR signaling.

The NER reaction generates ~30-nucleotide ssDNA gap intermediates by making dual incisions by XPF-ERCC1 (5′) and XPG (3′) endonucleases (17, 31–35). It might be possible that two events of dual incisions in close proximity on different DNA strands generates DSB, but this would be unlikely at UV doses used in this study, as discussed by others in detail (12). Another possibility is that some endonuclease(s) might be involved in the NER-dependent DSB formation. Similarly, it is plausible that NER-mediated ssDNA gaps in quiescent cells may need additional enzymatic processing to activate ATR for H2AX phosphorylation. In fact, ATR-mediated checkpoint activation has been shown to require the gap enlargement of NER intermediates by Exo1, using yeast Exo1 mutant (36), Exo1-down-regulated human cell lines (37), or more clearly a defined *in vitro* system (38). The mechanism underlying the NER-dependent DSB formation is currently unknown and awaits further study.

Cleaver and co-workers have reported that H2AX phosphorylation in cycling G_1 phase cells exposed to UV depends on NER but not DSB (12), although a minority of UV-induced γH2AX signal in S phase contains DSB (39). The NER-mediated DSB formation might be a specific or more frequent event in G_0 phase cells compared with cycling G_1 phase cells. In other words, quiescent cells need to activate not only NER but also other DDR pathways including ATR/ATM signaling and other DNA repair systems. Consistently, we found that functional ATM positively contributes to survival responses in quiescent cells exposed to UV (Fig. 4*C*).

The majority of *in vivo* cells are known to be nonproliferating or extremely slow to divide (*e.g.* terminally differentiated cells, tissue stem cells, and so on) (40). The NER-dependent H2AX phosphorylation can be observed after not only UV irradiation but also the treatment with *N*-acetoxy-2-acetylaminofluorene (14) or cisplatin[5] that produces bulky base adducts or intrastrand cross-links reparable by NER. The *in vivo* quiescent cells possibly suffer from the NER-mediated secondary DNA damage, in addition to initial base damage generated by UV or chemicals, and need to activate the multiple DDR mechanisms to prevent cell death or carcinogenic mutation.

Acknowledgments—We thank Dr. Kanji Ishizaki (Aichi Cancer Center Research Institute) for the hTERT-transformed cell lines and Dr. Toshio Mori (Nara Medical University) for XP2BI cells. We also thank Dr. Kuniyoshi Iwabuchi (Kanazawa Medical University) for anti-53BP1 antibody and Ai Igarashi for technical assistance.

REFERENCES

1. Sancar, A., Lindsey-Boltz, L. A., Unsal-Kaçmaz, K., and Linn, S. (2004) Molecular mechanisms of mammalian DNA repair and the DNA damage checkpoints. *Annu. Rev. Biochem.* **73,** 39–85
2. Ciccia, A., and Elledge, S. J. (2010) The DNA damage response: Making it safe to play with knives. *Mol. Cell* **40,** 179–204
3. Jackson, S. P., and Bartek, J. (2009) The DNA-damage response in human biology and disease. *Nature* **461,** 1071–1078
4. Downs, J. A., Nussenzweig, M. C., and Nussenzweig, A. (2007) Chromatin dynamics and the preservation of genetic information. *Nature* **447,** 951–958
5. van Attikum, H., and Gasser, S. (2009) Crosstalk between histone modifications during the DNA damage response. *Trends Cell Biol.* **19,** 207–217

6. Bonner, W. M., Redon, C. E., Dickey, J. S., Nakamura, A. J., Sedelnikova, O. A., Solier, S., and Pommier, Y. (2008) γH2AX and cancer. *Nat. Rev. Cancer* **8,** 957–967
7. Friedberg E. C., Walker G. C., Siede W., Wood R. D., Schultz R. A., and Ellenberger T. (2006) *DNA Repair and Mutagenesis,* ASM Press, Washington, D.C.
8. Ward, I. M., and Chen, J. (2001) Histone H2AX is phosphorylated in an ATR-dependent manner in response to replicational stress. *J. Biol. Chem.* **276,** 47759–47762
9. Cimprich, K. A., and Cortez, D. (2008) ATR: an essential regulator of genome integrity. *Nat. Rev. Mol. Cell Biol.* **9,** 616–627
10. Flynn, R. L., and Zou, L. (2011) ATR: a master conductor of cellular responses to DNA replication stress. *Trends Biochem. Sci.* **36,** 133–140
11. O'Driscoll, M., Ruiz-Perez, V. L., Woods, C. G., Jeggo, P. A., and Goodship, J. A. (2003) A splicing mutation affecting expression of ataxia-telangiectasia and Rad3-related protein (ATR) results in Seckel syndrome. *Nat. Genet.* **33,** 497–501
12. Marti, T. M., Hefner, E., Feeney, L., Natale, V., and Cleaver, J. E. (2006) H2AX phosphorylation within the G1 phase after UV irradiation depends on nucleotide excision repair and not DNA double-strand breaks. *Proc. Natl. Acad. Sci. U.S.A.* **103,** 9891–9896
13. Hanasoge, S., and Ljungman, M. (2007) H2AX phosphorylation after UV irradiation is triggered by DNA repair intermediates and is mediated by the ATR kinase. *Carcinogenesis* **28,** 2298–2304
14. Matsumoto, M., Yaginuma, K., Igarashi, A., Imura, M., Hasegawa, M., Iwabuchi, K., Date, T., Mori, T., Ishizaki, K., Yamashita, K., Inobe, M., and Matsunaga, T. (2007) Perturbed gap-filling synthesis in nucleotide excision repair causes histone H2AX phosphorylation in human quiescent cells. *J. Cell Sci.* **120,** 1104–1112
15. Vrouwe, M. G., Pines, A., Overmeer, R. M., Hanada, K., and Mullenders, L. H. (2011) UV-induced photolesions elicit ATR-kinase-dependent signaling in non-cycling cells through nucleotide excision repair-dependent and -independent pathways. *J. Cell Sci.* **124,** 435–446
16. Sancar, A. (1996) DNA excision repair. *Annu. Rev. Biochem.* **65,** 43–81
17. Huang, J.-C., Svoboda, D. L., Reardon, J. T., and Sancar, A. (1992) Human nucleotide excision nuclease removes thymine dimers from DNA by incising the 22nd phosphodiester bond 5′ and the 6th phosphodiester bond 3′ to the photodimer. *Proc. Natl. Acad. Sci. U.S.A.* **89,** 3664–3668
18. Wood, R. D. (1996) DNA repair in eukaryotes. *Annu. Rev. Biochem.* **65,** 135–167
19. Bootsma, D., Kraemer, K. H., Cleaver, J. E., and Hoeijmakers, J. H. J. (1998) Nucleotide excision repair syndromes: xeroderma pigmentosum, Cockayne syndrome and trichothiodystrophy. In *The Genetic Basis of Human Cancer* (Vogelstein, B., and Kinzler, K. W., eds) pp. 245–274, McGraw-Hill Inc., New York
20. Mori, T., Nakane, M., Hattori, T., Matsunaga, T., Ihara, M., and Nikaido, O. (1991) Simultaneous establishment of monoclonal antibodies specific for either cyclobutane pyrimidine dimer or (6-4)photoproduct from the same mouse immunized with ultraviolet-irradiated DNA. *Photochem. Photobiol.* **54,** 225–232
21. Bekker-Jensen, S., and Mailand, N. (2010) Assembly and function of DNA double-strand break repair foci in mammalian cells. *DNA Repair* **9,** 1219–1228
22. Nakamura, H., Fukami, H., Hayashi, Y., Kiyono, T., Nakatsugawa, S., Hamaguchi, M., and Ishizaki, K. (2002) Establishment of immortal normal and ataxia telangiectasia fibroblast cell lines by introduction of the hTERT gene. *J. Radiat. Res.* **43,** 167–174
23. Stiff, T., O'Driscoll, M., Rief, N., Iwabuchi, K., Löbrich, M., and Jeggo, P. A. (2004) ATM and DNA-PK function redundantly to phosphorylate H2AX after exposure to ionizing radiation. *Cancer Res.* **64,** 2390–2396
24. Suzuki, K., Kodama, S., and Watanabe, M. (1999) Recruitment of ATM protein to double strand DNA irradiated with ionizing radiation. *J. Biol. Chem.* **274,** 25571–25575
25. Stiff, T., Walker, S. A., Cerosaletti, K., Goodarzi, A. A., Petermann, E., Concannon, P., O'Driscoll, M., and Jeggo, P. A. (2006) ATR-dependent phosphorylation and activation of ATM in response to UV treatment or replication fork stalling. *EMBO J.* **25,** 5775–5782
26. Yajima, H., Lee, K. J., Zhang, S., Kobayashi, J., and Chen, B. (2009) DNA double-strand break formation upon UV-induced replication stress activates ATM and DNA-PKcs kinases. *J. Mol. Biol.* **385,** 800–810
27. Oh, K.-S., Bustin, M., Mazur, S. J., Appella, E., and Kraemer, K. H. (2011) UV-induced histone H2AX phosphorylation and DNA damage related proteins accumulate and persist in nucleotide excision repair-deficient XP-B cells. *DNA Repair* **10,** 5–15
28. Olson, E., Nievera, C. J., Lee, A. Y., Chen, L., and Wu, X. (2007) The Mre11-Rad50-Nbs1 complex acts both upstream and downstream of ataxia telangiectasia mutated and Rad3-related protein (ATR) to regulate the S-phase checkpoint following UV treatment. *J. Biol. Chem.* **282,** 22939–22952
29. Stiff, T., Cerosaletti, K., Concannon, P., O'Driscoll, M., and Jeggo, P. A. (2008) Replication independent ATR signaling leads to G2/M arrest requiring Nbs1, 53BP1 and MDC1. *Hum. Mol. Genet.* **17,** 3247–3253
30. Marteijn, J. A., Bekker-Jensen, S., Mailand, N., Lans, H., Schwertman, P., Gourdin, A. M., Dantuma, N. P., Lukas, J., and Vermeulen, W. (2009) Nucleotide excision repair-induced H2A ubiquitination is dependent on MDC1 and RNF8 and reveals a universal DNA damage response. *J. Cell Biol.* **186,** 835–847
31. O'Donovan, A., Davies, A. A., Moggs, J. G., West, S. C., and Wood, R. D. (1994) XPG endonuclease makes the 3′ incision in human DNA nucleotide excision repair. *Nature* **371,** 432–435
32. Matsunaga, T., Mu, D., Park, C.-H., Reardon, J. T., and Sancar, A. (1995) Human DNA repair excision nuclease analysis of the roles of the subunits involved in dual incisions by using anti-XPG and anti-ERCC1 antibodies. *J. Biol. Chem.* **270,** 20862–20869
33. Mu, D., Hsu, D. S., and Sancar, A. (1996) Reaction mechanism of human DNA repair excision nuclease. *J. Biol. Chem.* **271,** 8285–8294
34. Sijbers, A. M., de Laat, W. L., Ariza, R. R., Biggerstaff, M., Wei, Y. F., Moggs, J. G., Carter, K. C., Shell, B. K., Evans, E., de Jong, M. C., Rademakers, S., de Rooij, J., Jaspers, N. G., Hoeijmakers, J. H., and Wood, R. D. (1996) Xeroderma pigmentosum group F caused by a defect in a structure-specific DNA repair endonuclease. *Cell* **86,** 811–822
35. Reardon, J. T., Thompson, L. H., and Sancar, A. (1997) Rodent UV-sensitive mutant cell lines in complementation groups 6–10 have normal general excision repair activity. *Nucleic Acids Res.* **25,** 1015–1021
36. Giannattasio, M., Follonier, C., Tourrière, H., Puddu, F., Lazzaro, F., Pasero, P., Lopes, M., Plevani, P., and Muzi-Falconi, M. (2010) Exo1 competes with repair synthesis, converts NER intermediates to long ssDNA gaps, and promotes checkpoint activation. *Mol. Cell* **40,** 50–62
37. Sertic, S., Pizzi, S., Cloney, R., Lehmann, A. R., Marini, F., Plevani, P., and Muzi-Falconi, M. (2011) Human exonuclease 1 connects nucleotide excision repair (NER) processing with checkpoint activation in response to UV irradiation. *Proc. Natl. Acad. Sci. U.S.A.* **108,** 13647–13652
38. Lindsey-Boltz, L. A., Kemp, M. G., Reardon, J. T., DeRocco, V., Iyer, R. R., Modrich, P., and Sancar, A. (2014) Coupling of human DNA excision repair and the DNA damage checkpoint in a defined in vitro system. *J. Biol. Chem.* **289,** 5074–5082
39. de Feraudy, S., Revet, I., Bezrookove, V., Feeney, L., and Cleaver, J. (2010) A minority of foci or pan-nuclear apoptotic staining of γH2AX in the S phase after UV damage contain DNA double-strand breaks. *Proc. Natl. Acad. Sci. U.S.A.* **107,** 6870–6875
40. Pietras, E. M., Warr, M. R., and Passegué, E. (2011) Cell cycle regulation in hematopoietic stem cells. *J. Cell Biol.* **195,** 709–720

Mutagenesis vol. 29 no. 4 pp. 295–302
Advance Access publication 14 May 2014

doi:10.1093/mutage/geu018

Absence of *in vivo* genotoxicity of 3-monochloropropane-1,2-diol and associated fatty acid esters in a 4-week comprehensive toxicity study using F344 *gpt* delta rats

Saeko Onami[1,2], Young-man Cho[1], Takeshi Toyoda[1], Katsuyoshi Horibata[3], Yuji Ishii[1], Takashi Umemura[1,2], Masamitsu Honma[3], Takehiko Nohmi[3], Akiyoshi Nishikawa[2,4] and Kumiko Ogawa[1,*]

[1]Division of Pathology, National Institute of Health Sciences, 1-18-1 Kamiyoga, Setagaya-ku, Tokyo 158–8501, Japan, [2]Pathogenetic Veterinary Science, United Graduate School of Veterinary Sciences, Gifu University, 1-1 Yanagido, Gifu 501–1193, Japan, and [3]Division of Genetics and Mutagenesis and [4]Biological Safety Research Center, National Institute of Health Sciences, 1-18-1 Kamiyoga, Setagaya-ku, Tokyo 158–8501, Japan

*To whom correspondence should be addressed. Tel: +81 3 3700 9818; Fax: +81 3 3700 1425; Email: ogawa93@nihs.go.jp

Received on February 10, 2014; revised on April 4, 2014; accepted on April 7, 2014

3-Monochloropropane-1,2-diol (3-MCPD) is regarded as a rat renal and testicular carcinogen and has been classified as a possible human carcinogen (group 2B) by International Agency for Research on Cancer. This is potentially of great importance given that esters of this compound have recently found to be generated in many foods and food ingredients as a result of food processing. There have been a few reports about their toxicity, although we have recently found that the toxicity profile of 3-MCPD esters was similar to that of 3-MCPD in a rat 13-week repeated dose study, except for the acute renal toxicity seen in 3-MCPD-treated females. In the present study, to examine *in vivo* genotoxicity we administered equimolar doses of 3-MCPD or 3-MCPD fatty acid esters (palmitate diester, palmitate monoester and oleate diester) to 6-week-old male F344 *gpt* delta rats carrying a reporter transgene for 4 weeks by intragastric administration. *In vivo* micronucleus, *Pig-a* mutation and *gpt* assays were performed, as well as investigations of major toxicological parameters including histopathological features. As one result, the relative kidney weights of the 3-MCPD and all three ester groups were significantly increased compared with the vehicle control group. However, the frequency of micronucleated reticulocytes and *Pig-a* mutant red blood cells did not differ among groups. Moreover, no changes were observed in mutant frequencies of *gpt* and *red/gam* (Spi$^-$) genes in the kidney and the testis of 3-MCPD and 3-MCPD-fatty-acid-esters-treated rats. In histopathological analyses, no treatment related changes were observed, except for decrease of eosinophilic bodies in the kidneys of all treated groups. These results suggest that 3-MCPD and its fatty acid esters are not *in vivo* genotoxins, although they may exert renal toxicity.

Introduction

Genotoxicity assays have been used for screening carcinogenic potential of various agents. Although *in vitro* experiments can be readily and quickly performed, they may not reflect the absorption, distribution, metabolism and excretion of test compounds *in vivo*. Data from *in vivo* assays may have more relevance to effects in humans, including mechanisms of carcinogenesis. Therefore, the *in vivo* genotoxicity assays have been considered as important for risk assessment of new materials. Several *in vivo* genotoxicity assays have become established, each with a different endpoint. The *in vivo* micronucleus (MN) assay using peripheral blood or bone marrow cells obtained from rodents after single exposure of the test compound is widely accepted. It was also recommended by the International Conference on Harmonisation (ICH) guidelines as one of the genotoxicity testing battery required for the development of new drugs (1). This assay is used to detect damage to chromosomes or the mitotic apparatus. Substances that cause cytogenetic damage may give rise to cells with micronuclei, which consist of lagging chromosome fragments (a result of clastogenic activity) or whole chromosomes (due to aneugenic activity) (2).

In contrast to the MN assay, which generally is sensitive only to damage produced in a relatively small window of time before the sampling time, the *Pig-a* mutation assay can take advantage of the accumulative damage produced during an extended animal exposure (3). This assay is used to detect damage to the phosphatidylinositol glycan complementation class A (*Pig-a*) gene. The product of X-linked *Pig-a* gene is essential for synthesis of the glycosylphatidylinositol (GPI) anchor that links a specific subset of proteins to the cell surface. Therefore, mutations in the *Pig-a* gene can cause deficiencies of GPI-anchored proteins and GPI-anchored markers (4). The CD59 antigen is attached to the cytoplasmic membrane of erythroid cells *via* GPI anchors in the rat. In this assay, the frequency of mutant phenotype erythrocytes (RBC^{CD59-}) is determined via flow cytometric analysis.

The MN and *Pig-a* mutation assays are based on detecting DNA damage to haematopoietic cells as a result of systemic exposure. On the other hand, the *gpt* assay can detect point mutations and deletion mutations that escape from repair mechanisms and become fixed in target cells of carcinogens in rats and mice (5). This assay permits the efficient and quantitative detection of mutations in any tissue of rodents, with analyses of the mutations at the molecular level.

In the present study, we evaluated genotoxicty comprehensively using these three assays (MN, *Pig-a* mutation and *gpt* assays) for 3-monochloropropane-1,2-diol (3-MCPD) and three kinds of associated fatty acid esters.

3-MCPD is a food processing contaminant that belongs to a group of compounds called chloropropanols. It was first detected in acid-hydrolysed vegetable proteins (6). Further studies showed that 3-MCPD may also occur in other various products such as thermally processed foods like cereal-derived products (bread, biscuits), malt-derived products, coffee, cheese, smoked food, meat and salted fish (7, 8). Several *in vitro* and *in vivo* genotoxicity studies of 3-MCPD have been reviewed (9). *In vitro*, 3-MCPD induced reverse mutations in various strains of *Salmonella typhimurium* (10–12), and DNA

strand breaks in the comet assay with Chinese hamster ovary cells (13). On the other hand, no genotoxic effects of 3-MCPD were observed with the *in vivo* comet assay in various organs of SD and F344 rats (13), and there was no micronucleus formation in male Han Wistar rat bone marrow cells or unscheduled DNA synthesis in male Han Wistar rat hepatocytes (14).

In 2001, the Joint FAO/WHO Expert Committee on Food Additives established the provisional maximum tolerable daily intake (PMTDI) of 3-MCPD as 2 μg/kg body weight (B.W.)/day for human. This dose was based on the lowest observed effect level (LOEL) of 1.1 mg/kg B.W./day that induced renal tubular hyperplasia in a rat long-term study giving 3-MCPD by drinking water (15). The safety factor of 500 including additional factor of 5 for extrapolation from a LOEL to a no-observed-effect level (NOEL) was applied to establish the PMTDI (9). After rat carcinogenicity studies showed development of kidney and testicular carcinomas (15, 16), the International Agency for Research on Cancer classified 3-MCPD as a 'possible human carcinogen (group 2B)' (17).

Importantly, further analyses have revealed that 3-MCPD occurs in various foods either as a free form or more commonly esterified with long-chain fatty acids. High concentrations of 3-MCPD fatty acid esters have been reported in hydrogenated fats, palm oil and palm oil fractions solid frying fats (18,19). Moreover, occurrence of 3-MCPD fatty acid esters in human breast milk has been documented (20).

Recently, we conducted a rat 13-week subchronic toxicity study of three 3-MCPD fatty acid esters (palmitate diester: CDP, palmitate monoester: CMP, oleate diester: CDO) administered by gavage (21). Compared with 3-MCPD, the toxicities of the 3-MCPD fatty acid esters were lower in the acute phase regarding renal tubular necrosis and were equivalent in the subchronic phase, as evidenced by increase in male and female kidney weights and apoptosis in the initial segments of the epididymis. Liu *et al.* (22) also reported that renal tubular necrosis and protein casts in the kidneys were the major histopathological changes caused by acute oral toxicity of both CMP and CDP in Swiss mice. A 90-day toxicology study of 3-MCPD and CDP administered by daily oral gavage, conducted by Barocelli *et al.* (23), also revealed tubular epithelial hyperplasia or proliferation, basophilic or hyaline material and karyomegaly of tubular epithelial cells in CDP-treated rat kidneys.

For further risk assessment of 3-MCPD and 3-MCPD fatty acid esters, we here evaluated *in vivo* genotoxicity not only in haematopoietic cells but also in the potential target organs of carcinogenesis by *in vivo* MN, *Pig-a* mutation and *gpt* assays in male F344 *gpt* delta rats given these chemicals by gavage for 4 weeks.

Materials and methods

Test chemicals

Olive oil, 3-MCPD (98% pure), CDP (98% pure), (*sn1*)-CMP (1-palmitoyl-3-chloropropanediol; 98% pure) and CDO (98% pure) were purchased from Wako Pure Chemical Industries, Ltd (Osaka, Japan). Initially, (*sn2*)-CMP (2-palmitoyl-3-chloropropanediol) was also synthesised by Wako for analysis, but HPLC analysis revealed that (sn2)-CMP was unstable and spontaneously converting into (*sn1*)-CMP. For this reason, we analysed only (*sn1*)-CMP as a monoester.

Animals, diet and housing conditions

Six-week-old male F344 *gpt* delta rats carrying approximately 10 copies of the transgene lambda EG10 per haploid genome (24) were obtained from Japan SLC (Shizuoka, Japan). The animals were housed in polycarbonate cages (five or six rats per cage) with softwood chips for bedding in a specific pathogen-free animal facility, maintained under conditions of controlled temperature (23±2°C), humidity (55±5%), air change (12 times per hour) and lighting (12 h light/dark cycle) were given free access to a CRF-1 basal diet (Charles River Japan, Kanagawa, Japan) and tap water. The protocol for this study was approved by the Animal Care and Utilization Committee of the National Institute of Health Sciences.

Experimental design

After a 1-week acclimatisation period, 35 male F344 *gpt* delta rats weighing 82.2–117 g were used in this experiment. Rats were allocated with body-weight-basis randomisation to six groups consisting of five rats in the control group and six rats each in the olive oil (5 ml/kg B.W.), 3-MCPD (40 mg/kg B.W.) and 3-MCPD fatty acid ester groups (CDP: 220 mg/kg B.W., CMP: 130 mg/kg B.W. CDO: 240 mg/kg B.W.). The dose of 3-MCPD was selected based on previous carcinogenicity tests (16). Dose of 3-MCPD fatty acid esters was the same molar concentration of 3-MCPD. 3-MCPD and 3-MCPD fatty acid esters were dissolved in olive oil at the time of dosing and administered 5 times a week by intragastric tube for 4 weeks. The animals were observed daily for any clinical signs and mortality. Body weights were measured weekly. For *Pig-a* mutation assay, peripheral blood samples were collected from the tail vein of each animal (five per group) at Day 0 (before the first administration) and 15 (2 weeks after start of administration). At Day 29, after an overnight fast, within 24 h after the final administration, all the animals were anaesthetised with isoflurane, weighed blood samples were collected from the abdominal aorta for serum biochemistry and *Pig-a* mutation assays. The animals were then sacrificed by exsanguination from the abdominal aorta. For the *Pig-a* mutation assay, 9 μl whole blood samples were transferred to tubes and the remaining blood samples were left out to clot at room temperature for 30 min. After centrifugation at 3000 rpm for 10 min, the resultant sera were stored at −20°C until shipping for analysis.

Histopathology

The liver, kidneys and spleen were weighed and relative organ weights were calculated as the ratios between organ and body weights. The right kidney and testis were stored at −80°C for *gpt* assays. In addition, the liver, left kidney, spleen and left testis were fixed in 10% neutral buffered formalin embedded in paraffin, sectioned to a thickness of 3 μm stained with haematoxylin and eosin (HE) for microscopic examination. Kidney sections were also stained with PAS and Masson's trichrome staining. Histopathological examinations were carried out for all animals. Those found dead were also analysed as far as possible.

Serum biochemistry

The frozen serum samples were packed with dry ice and shipped within a few hours to SRL, Inc (Tokyo, Japan) where the parameters for serum biochemistry shown in Table II were analysed.

Micronucleus assays

For the Micronucleus (MN) assays, proximal and distal ends of the left femurs were cut and syringes with 23G needles were used to flush the bone marrow tissue with 0.5 ml foetal bovine serum (FBS) into 1.5 ml tubes. Cell suspensions kept on ice were centrifuged at 1000 rpm for 5 min and cell pellets were re-suspended in almost the same volume of FBS using Pasteur pipettes. Aliquots of 5 μL of cell suspension were spread on standard microscope slides. After air-drying for overnight, these smear slides were fixed with absolute methanol for 10 min and stored in a slide box until staining with acridine orange (Wako Pure Chemical Industries, Ltd.) and washing with phosphate buffer (pH 6.8). Micronuclei were immediately counted per at least 2000 reticulocytes (RETs) per animal using a fluorescence microscope. In addition, at least 1000 erythrocytes (RETs and mature) were scored to determine %RETs as a measure of chemical-induced bone marrow toxicity.

Pig-a *mutation assays*

Peripheral blood collection and staining of total red blood cells (RBCs) were conducted according to the previous report with slight modifications (25). Peripheral blood samples of 9 μl were promptly mixed with 1 μl of 12 mg/ml K_2-EDTA. Three microlitres of blood/EDTA mixture were suspended in 200 μL of phosphate-buffered saline (PBS) the cells were labelled with 1 μg of FITC-conjugated anti-rat CD59 (BD Biosciences, Tokyo, Japan) and 0.125 μg of biotinylated HIS49 antibody (erythroid marker; BD Biosciences). After incubation for 1 h in the dark at room temperature, the samples were washed with PBS, centrifuged for 5 min at 1000 g re-suspended in 200 μL of PBS. Then the samples were mixed with 0.2 μg of APC-conjugated streptavidin (BD Biosciences) and incubated for 15 min in the dark at room temperature. They were finally centrifuged for 5 min at 1000 g and re-suspended in 1 mL of PBS. The frequency of *Pig-a* mutant RBCs was determined as the number of RBC^{CD59-} per 1 million total RBCs using a FACS Canto II flow cytometre (BD Bioscience). For determinations of the

frequency of RBC^{CD59-}, single cells, including RBCs and white blood cells, were gated by light scatter. HIS-49-positive cells from this population were analysed further for the presence of the GPI-anchored CD59 antigen on the cell surface.

gpt *assays*

Following the method of Nohmi *et al.* (5), 6-thioguanine (6-TG) and Spi^- selections were performed. Briefly, genomic DNA was extracted from the kidney and testis, reported as target organs of 3-MCPD (15, 16), and lambda EG10 DNA (48 kb) was rescued as phages by *in vitro* packaging. For 6-TG selection, packaged phages were incubated with *Escherichia coli* YG6020, which expresses *Cre* recombinase converted to plasmids carrying the *gpt* and chloramphenicol acetyltransferase genes. In order to determine the ratio of mutation-carrying plasmids, infected cells were mixed with molten soft agar and poured onto agar plates containing chloramphenicol with/without 6-TG. The plates were then incubated at 37°C for selection of 6-TG-resistant colonies the *gpt* mutant frequency (MF) was calculated by dividing the number of *gpt* mutants after clonal correction for the number of rescued phages. *gpt* mutations were characterised by amplifying a 739-bp DNA fragment containing the 456-bp coding region of the *gpt* gene (5). For Spi^- selection, packaged phages were incubated with E. coli XL-1 Blue MRA for survival titration and E. coli XL-1 Blue MRA P2 for mutant selection. Infected cells were mixed with molten lambda-trypticase agar plates. The next day, plaques (Spi^- candidates) were punched out with sterilised glass pipettes and the agar plugs were suspended in sucrose mannitol buffer. The Spi phenotype was confirmed by spotting the suspensions on three types of plates where XL-1 Blue MRA, XL-1 Blue MRA P2, or WL95 P2 strains were spread with soft agar. Spi^- mutants, which made clear plaques on every plate, were counted. To confirm the efficacy of the procedure for the *gpt* assay, positive DNA samples extracted from rat liver treated with a known genotoxic hepatocarcinogen, diethylnitrosamine (DEN), were also assessed.

Statistical analysis

Variance in the data for body weights, organ weights, serum biochemistry, frequencies of MN-RETs, percent RETs among total erythrocytes and frequencies of RBC^{CD59-} was checked for homogeneity by Bartlett's procedure. When the data were homogeneous, one-way analysis of variance was applied. In the heterogeneous cases, the Kruskal–Wallis test was used. When statistically significant differences were indicated, Dunnett's multiple test was employed for comparison between olive oil and treated groups. P values less than 0.05 were considered statistically significant in both analyses.

Results

General conditions

Body weights. Three rats, one each treated with CDP, CMP or CDO died with haemorrhage of the oesophagus–thoracic cavity without histological change of kidneys, the cause being accidental related to gavage problems. There was no deterioration in the general conditions observed in any of the groups. The body weights of all groups increased gradually and progressively with age. No significant differences in body weight gain were detected among treatment groups (Figure 1).

Organ weights

Final body weights and the absolute and relative organ weights are shown in Table I. Compared with vehicle control group, significant increase in absolute and relative kidney weights

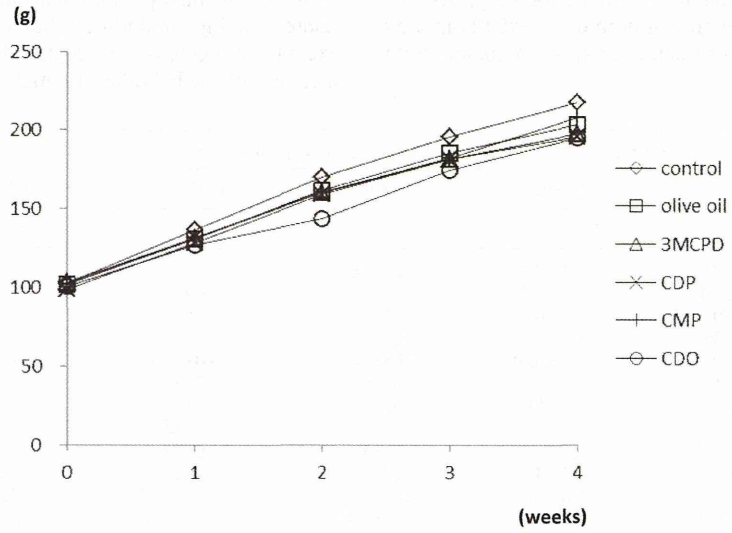

Fig. 1. Body weight curves for F344 *gpt* delta rats treated with 3-MCPD fatty acid esters for 4 weeks.

Table I. Organ weight for F344 *gpt* delta rats treated with 3-MCPD fatty acid esters for 4 weeks

Treatment	Control	Olive oil	3-MCPD	CDP	CMP	CDO
No. of animals	5	6	6	5	5	5
Body weight (g)	218±23	203±10	197±13	196±14	208±11	195±11
Absolute						
Spleen (g)	0.49±0.04	0.46±0.03	0.5±0.04	0.47±0.03	0.5±0.04	0.48±0.02
Liver (g)	8.4±1	7.4±0.5	7.5±0.5	7.7±0.9	8.1±0.6	7.6±0.3
Kidneys (g)	1.6±0.15	1.4±0.1	1.6±0.12*	1.7±0.10**	1.7±0.07**	1.7±0.06**
Relative						
Spleen (%)	0.23±0.013	0.23±0.01	0.25±0.009**	0.24±0.004	0.24±0.017	0.25±0.006*
Liver (%)	3.9±0.2	3.7±0.1	3.8±0.1	3.9±0.2	3.9±0.1	3.9±0.2
Kidneys (%)	0.72±0.02	0.69±0.04	0.81±0.03**	0.87±0.02**	0.83±0.04**	0.86±0.02**

Each value represents the mean ± SD.
Significantly different from the olive oil group at $*P < 0.05$ and $**P < 0.01$.

was noted in the 3-MCPD, CDP, CMP and CDO groups. With spleen, only relative weights were increased in the 3-MCPD and CDO groups.

Serum biochemistry

The results of serum biochemical analysis are summarised in Table II. Compared with the vehicle control group, significant increases in glucose of all 3-MCPD fatty acid ester groups and inorganic phosphorus (IP) of the CMP and CDO groups were observed. Significant decrease in aspartate aminotransferase (AST) of the CMP and CDO groups and creatinine (Cre) of the 3-MCPD and all 3-MCPD fatty acid ester groups was also noted.

Histopathology

Eosinophilic bodies, negative for PAS reaction and positively stained with Masson's trichrome staining (data not shown), seen in the renal proximal tubular epithelium were decreased in the 3-MCPD fatty acid ester groups compared with control and olive oil groups (Table III and Figure 2). No treatment-related changes were observed in the liver, spleen and testis.

MN assay

The frequency of micronucleated reticulocytes (MN-RETs) (Figure 3A) and the percentage RETs among total erythrocytes (Figure 3B) did not differ significantly in the 3-MCPD-treated and 3-MCPD-fatty-acid-ester-treated groups compared with the control groups.

Pig-a *mutation assay*

The frequency of *Pig-a* mutant RBCs did not differ among groups at any time point (Figure 4).

gpt *assay*

In the samples from the DEN-treated liver performed as the positive control, the MFs of *gpt* (more than 40-folds) and of Spi$^-$ (more than 5-folds) were significantly elevated (data not shown), MFs in the kidney and testis in the 3-MCPD and its ester-treated groups (Figure 5) were within background levels reported previously (26). There were no significant differences in the *gpt* MFs as well as Spi$^-$ MFs among the groups.

Discussion

The results of the present study do not provide any evidence that 3-MCPD or the esters exert genotoxity or other major toxicity.

In organ weight data, the absolute and relative kidney weights in the 3-MCPD, CDP, CMP and CDO groups were significantly increased. This change was observed in our previous 13-week study of these chemicals in both male and female wild F344 rats (21), and in other groups' 13-week studies of 3-MCPD in B6C3F1 mice (27) and of 3-MCPD or CDP in Wistar rats (23). However, in histopathological analysis of kidney, treatment-related findings including tubular necrosis were not observed, except for decrease of eosinophilic bodies. In general, an increase of such bodies in male rat kidney has rather been

Table II. Serum biochemistry for F344 *gpt* delta rats treated with 3-MCPD fatty acid esters for 4 weeks

Treatment	Control	Olive oil	3-MCPD	CDP	CMP	CDO
No. of animals	5	6	6	5	5	5
TP (g/dL)	6.1±0.2	6.1±0.2	5.9±0.2	5.8±0.2	5.9±0.1	5.8±0.1
Alb (g/dL)	4±0.1	4.1±0.2	4±0.1	3.9±0.2	4±0.1	4±0.1
A/G	1.9±0.1	2.1±0.2	2.2±0.1	2.1±0.4	2.2±0.1	2.2±0.1
Glucose (mg/dL)	183±39	169±27	168±21	219±25**	228±16**	248±12**
Bil (mg/dL)	0.03±0.01	0.03±0.01	0.03±0.01	0.02±0.01	0.03±0	0.03±0.01
T-Cho (mg/dL)	65±5	54±4	54±3	57±8	55±5	57±3
TG (mg/dL)	191±18	117±51	68±24	67±26	96±34	88±23
γGTP (IU/L)	<3	<3	<3	<3	<3	<3
AST (IU/L)	87±13	85±10	74±6	65±6	62±1*	59±5**
ALT (IU/L)	33±3	32±4	29±1	28±4	29±2	28±1
ALP (IU/L)	1152±73	1336±91	1275±111	1190±233	1233±98	1229±117
BUN (mg/dL)	18.7±1.9	14.2±2.2	11.3±1.0*	11.7±1.2	12.8±1.5	12.7±1.7
Cre (mg/dL)	0.28±0.01	0.27±0.02	0.23±0.01**	0.22±0.01**	0.22±0.01**	0.22±0.02**
Ca (mg/dL)	10.2±0.2	10.3±0.3	10.2±0.2	10.2±0.1	10.2±0.1	10.3±0.2
IP (mg/dL)	6.1±0.2	5.9±0.2	6.9±0.4	6.7±0.9	7.1±0.5*	7.2±0.3*
Na (mg/dL)	141±2	143±3	143±1	142±1	141±1	141±1
K (mg/dL)	4.7±0.2	4.3±0.2	4.5±0.2	4.2±0.1	4.3±0.4	4.5±0.2
Cl (mg/dL)	100±1	102±2	104±1	103±2	102±1	101±2

Each value represents the mean ± SD. TP, total protein; Alb, albumin; Bil, bilirubin; T-Cho, total cholesterol; AST, aspartate aminotransferase; ALT, alanine aminotransferase; ALP, alkaline phosphatase; BUN, blood urea nitrogen; Cre, creatinine.
Significantly different from the olive oil group at $^*P < 0.05$ and $^{**}P < 0.01$.

Table III. Histopathological change in kidney for F344 *gpt* delta rats treated with 3-MCPD fatty acid esters for 4 weeks

	Control	Olive oil	3-MCPD	CPD	CPM	CDO
No. of rats examined	5	6	6	5	5	5
Eosinophilic body, cortex, proximal tubular (−/±/+)[a]	0/1/4	0/4/2	6/0/0	5/0/0	5/0/0	5/0/0

[a]Ratio of proximal tubules with eosinophilic body :− < 5%, ± < 25%, + < 50%.

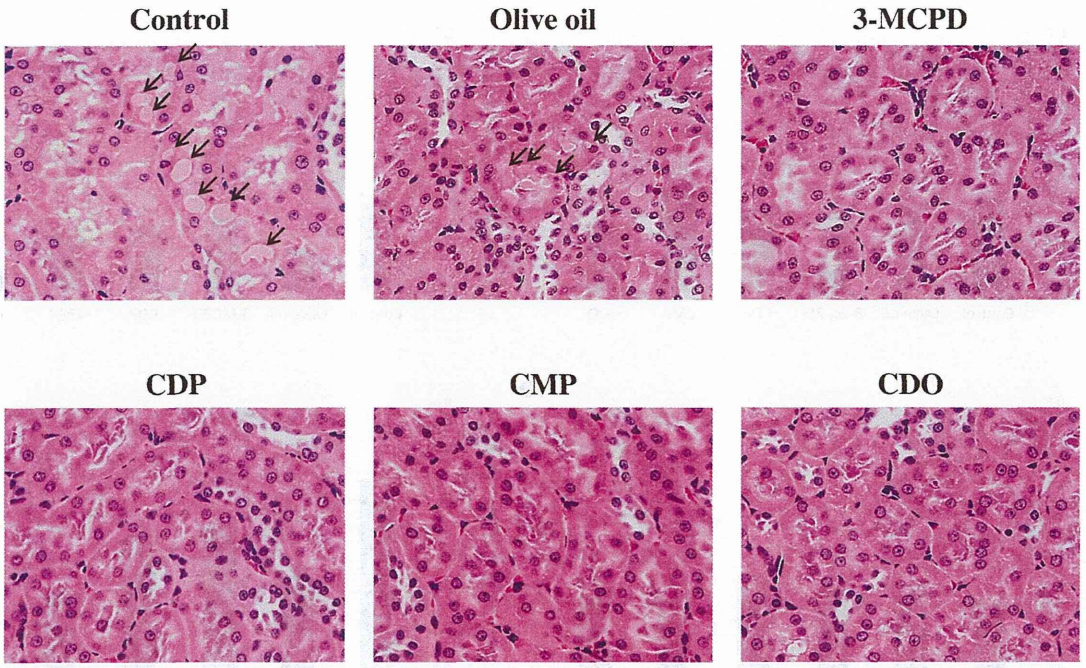

Fig. 2. Photomicrograph of kidneys of F344 *gpt* delta rats (HE staining). Black arrows indicate eosinophilic bodies in the renal proximal tubular epithelium in control and olive oil groups.

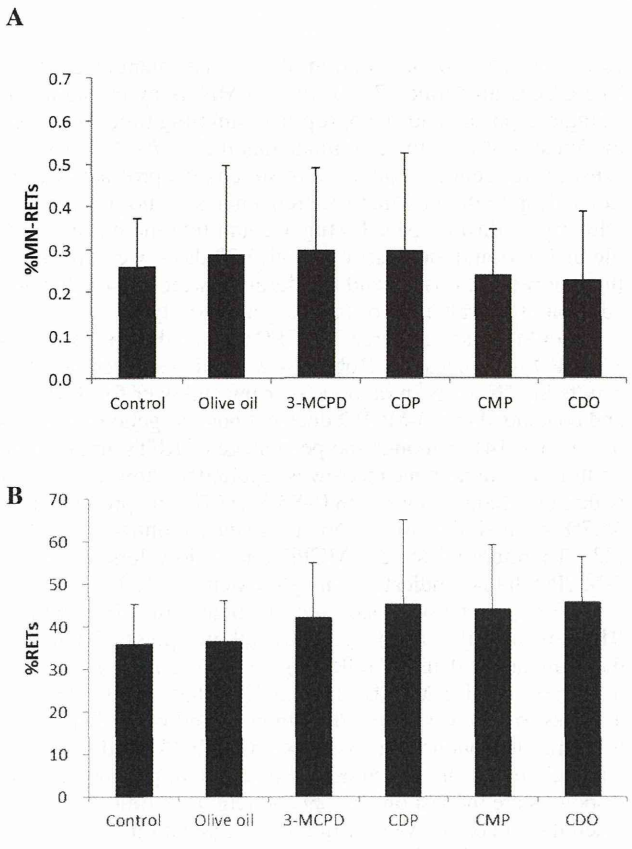

Fig. 3. (**A**) Frequency of MN-RETs in rat bone marrow after 4 weeks treatment. (**B**) Percentage RETs among total erythrocytes in rat bone marrow after 4 weeks treatment. The values represent the means of experiments ± standard deviations.

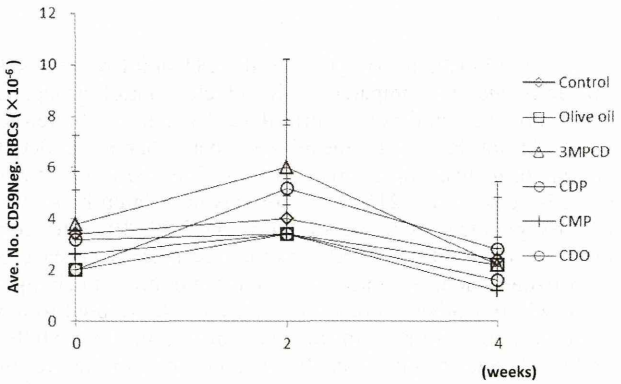

Fig. 4. Average frequencies of RBC^{CD59-} following treatment of F344 *gpt* delta rats for 4 weeks. The values represent the means of experiments ± standard deviations.

reported as an adverse change associated with the accumulation of alpha 2u-globulin, a male-specific protein synthesised in the liver (28,29). No significant change in serum biochemical analysis related to liver toxicity was confirmed. Furthermore, any toxicological implication of decrease of eosinophilic bodies in kidney has not been elucidated. Although the mode of action was not clear, it was confirmed that the increase of the absolute and relative kidney weight indicated the renal effects of 3-MCPD and its fatty acid esters in the present 4 weeks *gpt* delta rat study.

The relative spleen weight increased in 3-MCPD and CDO groups but the absolute spleen weight did not change. The difference was about 10% and there were no significant histological lesions in the spleens of these groups. Therefore, the relative spleen weight changes were considered as incidental.